Oxygen Evolution Reaction Hot Paper

International Edition: DOI: 10.1002/anie.201502226
German Edition: DOI: 10.1002/ange.201502226

Ultrathin Spinel-Structured Nanosheets Rich in Oxygen Deficiencies for Enhanced Electrocatalytic Water Oxidation**

Jian Bao, Xiaodong Zhang, Bo Fan, Jiajia Zhang, Min Zhou, Wenlong Yang, Xin Hu, Hui Wang, Bicai Pan, and Yi Xie**

Abstract: *Electrochemical water splitting is a clean technology for H_2 fuels, but greatly hindered by the slow kinetics of the oxygen evolution reaction (OER). Herein, a series of spinel-structured nanosheets with oxygen deficiencies and ultrathin thicknesses were designed to increase the reactivity and the number of active sites of the catalysts, which were then taken as an excellent platform for promoting the water oxidation process. Theoretical investigations showed that the oxygen vacancies confined in the ultrathin nanosheet could lower the adsorption energy of H_2O, leading to increased OER efficiency. As expected, the $NiCo_2O_4$ ultrathin nanosheets rich in oxygen vacancies exhibited a large current density of 285 mA cm^{-2} at 0.8 V and a small overpotential of 0.32 V, both of which are superior to the corresponding values of bulk samples or samples with few oxygen deficiencies and even higher than those of most reported non-precious-metal catalysts. This work should provide a new pathway for the design of advanced OER catalysts.*

Electrochemical and photochemical water splitting have been regarded as promising approaches for energy storage and conversion and utilize electric energy to split abundant water into clean H_2 fuel.[1–4] Among the electrochemical processes, the oxygen evolution reaction (OER) is efficiency-limiting owing to the complex four-electron redox process, and thus hinders the large-scale application of electrochemical water splitting.[5–7] Generally speaking, an appropriate OER catalyst is required to address the kinetically slow process. Among all tested candidates, ruthenium and iridium oxides are known to exhibit the best overall performances but their use is limited by their scarcity and high cost.[8,9] Accordingly, much efforts have been devoted to searching for alternative OER electrocatalysts that are based on abundant and economic 3d metals and their derivatives.[10–15] Among these non-precious-metal catalysts, spinel-structured oxides, with their high electronic conductivity and stability, have exhibited a superior performance in the OER. However, their electrocatalytic performance is still far from the requirements of practical applications. The design of simple and economic alternative routes to obtain highly active non-precious-metal catalysts will be key for the development of electrocatalytic water oxidation.

Active sites play the key role in catalytic processes. Therefore, increasing the reactivity and number of active sites will be two effective ways to enhance electrocatalytic performance. As a promising structural motif for realizing a great number of active sites, two-dimensional (2D) nanosheets with ultrathin thickness possess the maximum number of electroactive surface/active sites, which can also lead to a decrease in the length of the diffusion paths of ions and an increase in the contact area with the electrolyte. Such materials are thus suitable candidates for the realization of highly efficient catalysts for electrochemical processes.[16–18]

Apart from the electroactive surface area, the reactivity of active sites, which is associated with the interaction between the catalyst surface and O_2/H_2O, also plays an important role in the OER process. Nowadays, research is mainly focused on the role that active metal atoms play in the OER performance, whereas attention is rarely paid to the non-metal atoms.[8] For example, in the spinel structure, the active sites are considered to be octahedral cobalt centers in the form of Co_4O_4 cubanes.[19] However, oxygen vacancies, which also have an influence on the OER, have often been ignored in studying the OER despite the wide attention that they have received in other electrochemical systems, such as lithium batteries and solid-oxide fuel cells.[20]

It is well known that H_2O molecules are initially adsorbed onto the surface of the catalyst during the OER process. The reaction then proceeds according to the following mechanism:

$$2\,H_2O + * \rightarrow OH^* + H_2O + e^- + H^+ \quad (1)$$

$$OH^* + H_2O \rightarrow O^* + H_2O + e^- + H^+ \quad (2)$$

$$O^* + H_2O \rightarrow OOH^* + e^- + H^+ \quad (3)$$

$$OOH^* \rightarrow O_2 + e^- + H^+ \quad (4)$$

[*] J. Bao, Dr. X. D. Zhang, B. Fan, J. J. Zhang, W. L. Yang, X. Hu, H. Wang, Prof. B. C. Pan, Prof. Y. Xie
Hefei National Laboratory for Physical Science at the Microscale
Collaborative Innovation Center of Chemistry for Energy Materials
University of Science and Technology of China
Hefei, Anhui, 230026 (P. R. China)
E-mail: zhxid@ustc.edu.cn
yxie@ustc.edu.cn
Dr. M. Zhou
Institute of Physics and IMN MacroNano (ZIK)
Ilmenau University of Technology
98693 Ilmenau (Germany)

[**] The project was supported by the National Basic Research Program of China (2015CB932302), the National Natural Science Foundation of China (21331005, 11321503, 21401181, and 91422303), the China Postdoctoral Science Foundation (BH2060140013), and the Fundamental Research Funds for the Central University (WK2060190032, WK2060190027, and WK2340000063). The supercomputer center of USTC is acknowledged for computational support.

Supporting information for this article is available on the WWW under http://dx.doi.org/10.1002/anie.201502226.

In that case, the adsorption energy of H_2O molecules onto the active sites plays a crucial role in the OER activity of the catalyst materials, as the adsorption is a rate-determining process.[21] To understand the contribution of the oxygen vacancies, we performed DFT modeling, which is a useful method for elucidating the OER process. Taking $NiCo_2O_4$, a most promising OER candidate, as an example, two models with a perfect surface or a surface with one oxygen vacancy were constructed. As show in Figure 1, the existence of an

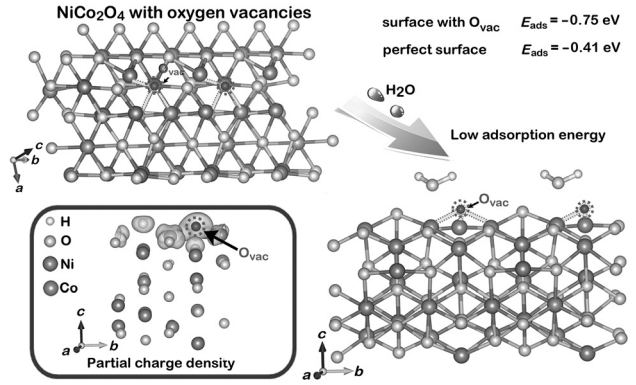

Figure 1. Schematic illustration of the adsorption of H_2O molecules onto the spinel structure and the partial charge density of $NiCo_2O_4$ with oxygen vacancies.

oxygen vacancy could decrease the hindrance for the adsorption of H_2O as the adsorption of H_2O at a Co^{3+} site is more favorable for low-coordination sites.[8] Moreover, as can be seen from the partial charge density of a $NiCo_2O_4$ sample with oxygen vacancies in Figure 1, in a surface with oxygen vacancies, the electrons neighboring the oxygen vacancy that previously occupied the O 2p orbital become delocalized, suggesting that a surface with oxygen vacancies is much more activated. Therefore, a Co^{3+} center, which tends to be octahedrally coordinated, is more active towards the adsorption of H_2O near an oxygen vacancy in the surface to achieve a coordination number of six than in a surface without oxygen vacancies. DFT calculations were carried out to study the adsorption energy of H_2O molecules on the nanosheet surfaces. The adsorption energy for a surface with one oxygen vacancy is –0.75 eV, which is lower than that of the perfect surface (–0.41 eV; Figure 1). Therefore, we can deduce that the oxygen vacancies promote the adsorption of H_2O molecules onto the surface of the catalysts, which is valuable for increasing the reactivity of active sites and the OER performance. Furthermore, the delocalized electrons around an oxygen vacancy are easy to be excited to the conduction band, which enhances the conductivity of $NiCo_2O_4$.[12] Bearing the above discussion in mind, herein, ultrathin spinel-structured nanosheets with oxygen vacancies are first put forward as an ideal material for investigating the effect of oxygen vacancies on the OER processes.

In this study, state-of-the-art $NiCo_2O_4$ ultrathin nanosheets rich in vacancies were synthesized through topochemical transformations from few-layered NiCo hydroxides. The as-obtained product was fabricated into a film by a layer-by-layer assembly strategy. When analyzed by X-ray diffraction (XRD; Figure 2A), the phase of the film could be indexed to spinel-structured $NiCo_2O_4$ (JCPDS 73-1702) and demonstrated a (222) preferential orientation. The TEM image in Figure 2B shows that the as-obtained sample possesses a sheet-like morphology with a size of about 150 nm, while the near transparency of the sheet indicates its ultrathin thickness. Microscopically, the colloidal suspension of the product displays the Tyndall phenomenon (Figure 2B, inset), so that the formation of homogeneous ultrathin nanosheets in water can be inferred.[22] The thickness of the as-prepared nanosheets was further studied by atomic force microscopy (AFM). As shown in Figure 2C and D, the height of the nanosheets is approximately 1.6 nm, which is about twice the value of 0.8 nm for the unit-cell dimensions given for $NiCo_2O_4$ (JCPDS 73-1702).[23] All of the results undoubtedly confirm that $NiCo_2O_4$ nanosheets with ultrathin thickness have been successfully synthesized.

As mentioned, oxygen vacancies play an important role in the OER. Herein, we obtained ultrathin nanosheets that are rich or poor in oxygen vacancies by calcining the corresponding NiCo hydroxides in air or oxygen atmosphere, to obtain NiCo-r and NiCo-p nanosheets, respectively. The deficiencies in the as-obtained ultrathin nanosheets and the corresponding bulk samples were then studied by X-ray photoelectron spectroscopy (XPS). As deduced from the relative intensities of the Co^{3+} and Co^{2+} peaks in the Co 2p core level spectra (Figure 2E), the majority of cobalt atoms in the crystal lattice are present as Co^{3+} cations.[24,25] In the O 1s core level spectra, three peaks can be clearly identified (Figure 2F). In detail, the peak at 529.7 eV is due to oxygen atoms bound to metals,[26,27] the peak at 532.6 eV is associated with hydroxy species of surface-adsorbed water molecules,[28] and the peak at 531.2 eV is attributed to a high number of defect sites with a low oxygen coordination.[29] The area of the peak at 531.2 eV is largest for the NiCo-r nanosheet among the three samples, which indicates that the ultrathin $NiCo_2O_4$ nanosheets obtained in air possess many more oxygen vacancies than the other counterparts. This finding could be further confirmed by photoluminescence spectroscopy of the samples (Figure S5), as the $NiCo_2O_4$ nanosheets obtained in air showed the highest luminescence intensity. The successful synthesis of samples that are rich or poor in vacancies provides ideal models to study the relationship between oxygen vacancies and the OER process.

To shed light on the role that oxygen vacancies play in the OER, the obtained ultrathin $NiCo_2O_4$ nanosheets that are rich or poor in oxygen vacancies as well as bulk samples were tested in the electrochemical OER in 1M KOH solutions. The overpotential that is required to achieve a current density of 10 mA cm^{-2} is a metric relevant to solar fuel production. Herein, as shown in Figure 3A, the ultrathin NiCo-r sample gave an overpotential (η) of 0.32 V, which is the smallest value for the three samples. Furthermore, the ultrathin NiCo-r nanosheets exhibited a very large anodic current density of 285 mA cm^{-2} at 0.8 V, which is 2.3 times larger than that of the ultrathin NiCo-p nanosheets. Moreover, the corresponding

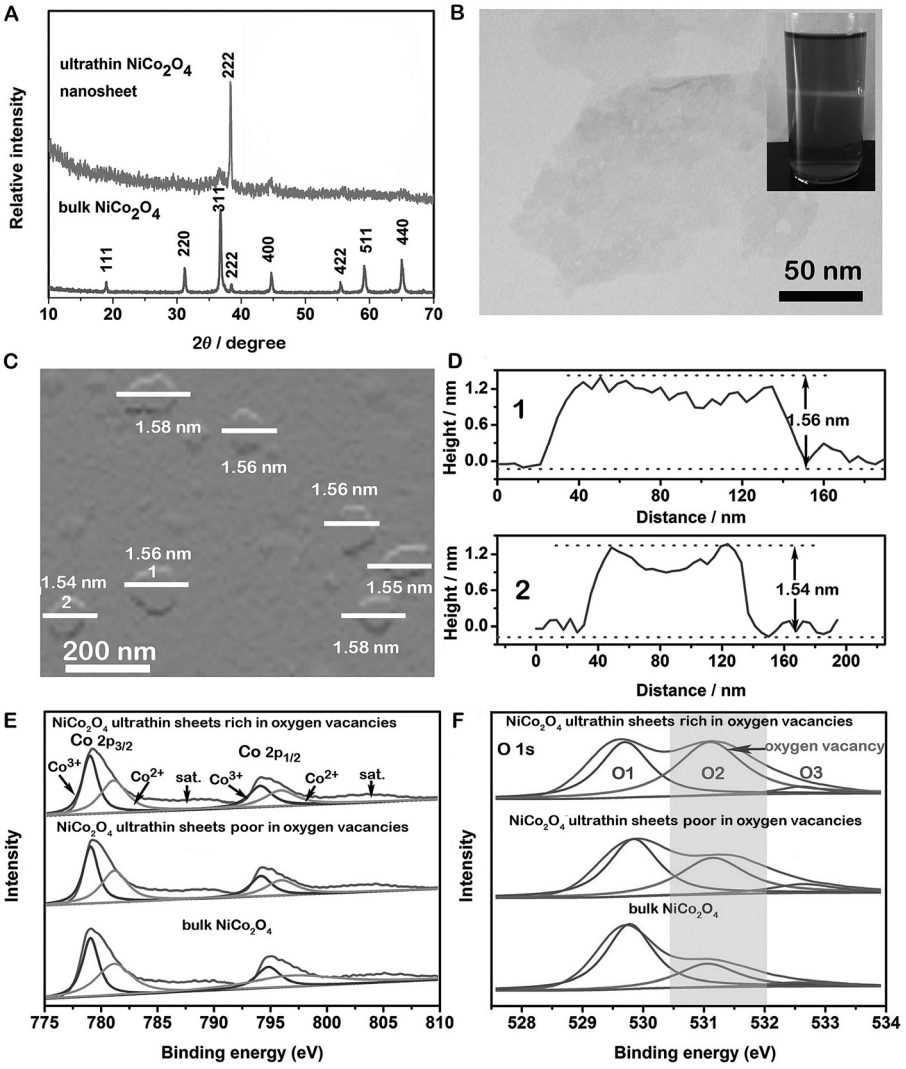

Figure 2. A) XRD patterns of the as-obtained $NiCo_2O_4$ nanosheets rich in oxygen vacancies and bulk $NiCo_2O_4$. B) TEM image of a freestanding nanosheet of $NiCo_2O_4$ and photograph of the corresponding colloidal dispersion displaying the Tyndall effect (inset). C) AFM image and D) corresponding height profile of the as-obtained nanosheet. E) The Co 2p spectra and F) O 1s spectra of the samples.

Tafel plots (Figure 3B) indicate that the ultrathin NiCo-r sample possesses smaller Tafel slopes (30 mV decade^{-1}) than NiCo-p and the bulk sample (54 and 57 mV decade^{-1}, respectively). A smaller Tafel slope is more beneficial for practical applications as it leads to a remarkably increased OER rate with an increase in overpotential. All of the above results indicate the important role of oxygen vacancies in the OER process.

To further investigate the effects of ultrathin thickness and oxygen vacancies, the capacitance of each oxide–solution interface and the roughness factors of the NiCo samples were estimated. As shown in Figure 3C, the current densities were measured from 0.5 mV s^{-1} to 9 mV s^{-1} at 0.24 V and can be plotted as a function of the sweep rate to study the effective surface area of the $NiCo_2O_4$ samples by evaluating the electrochemical double-layer capacitance (C_{dl}) and roughness factor (R_f). As expected, the NiCo-r ultrathin nanosheets exhibit the largest C_{dl} and R_f values among the three samples (30.8 mF cm^{-2} and 513, respectively), revealing that its active sites are the most effective. As can be deduced from Figure 3D, the R_f values of both NiCo-r and NiCo-p are approximately 40–50 times larger than that of the bulk sample, which further confirms the importance of the ultrathin 2D structure for the catalyst performance and for the enhanced electroactivity of the surfaces. Moreover, although the R_f values of the ultrathin nanosheets that are rich or poor in oxygen vacancies are similar to each other, the catalytic activities of the two samples are dramatically different, which could be attributed to their different oxygen vacancy concentrations.

The kinetics of the catalytic processes on the $NiCo_2O_4$ samples were examined by electrical impedance spectroscopy (EIS; Figure 3E) to further illustrate the superior OER performance of the NiCo-r nanosheets. Compared to the other two samples, the NiCo-r ultrathin nanosheets have the lowest charge-transfer resistance of 9.5 Ω, indicating its superior charge transport kinetics.[30] This result is due to synergistic effects between the ultrathin thickness and the oxygen vacancies, which lead to intimate contact with the GC electrode, a high interfacial contact area with the electrolyte, short ion diffusion paths, and the fast adsorption of H_2O molecules, and thus accelerate charge transport. Aside from the OER activity, stability is another crucial factor to evaluate an advanced electrocatalyst. As shown in Figure 3F for the long-term cycling stability of a NiCo-r sample, negligible differences can be observed even after 1000 CV cycles, revealing the excellent durability of the ultrathin nanosheets.

To further confirm the positive effect of the oxygen vacancies on the OER process, other ultrathin nanosheets, such as $ZnCo_2O_4$ and Co_3O_4 nanosheets, that were rich and poor in vacancies were also synthesized and studied as OER catalysts. As shown in Figure 4, all samples that are rich in oxygen vacancies showed a lower overpotential, smaller Tafel slopes, higher current densities as well as larger TOF values than the corresponding samples that are poor in oxygen vacancies, demonstrating the important role of oxygen vacancies in the OER process. Moreover, the $NiCo_2O_4$ ultrathin nanosheets that are rich in oxygen vacancies also

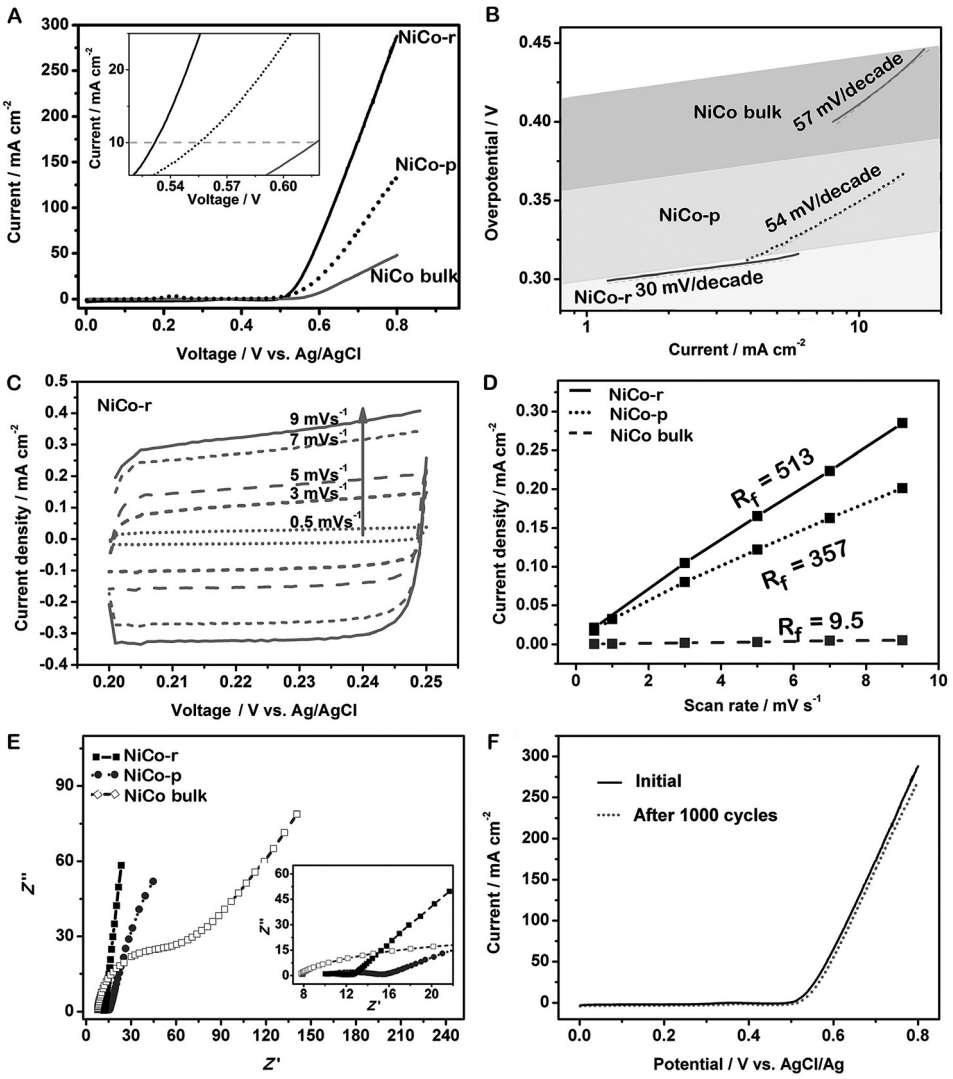

Figure 3. A) Polarization curves of the various $NiCo_2O_4$ samples. Inset: enlargement of the region near the onset. B) Corresponding Tafel plots of the samples. C) CVs of the NiCo-r electrode measured in 1 M KOH solution at scan rates from 0.5 to 9 $mV s^{-1}$. D) Current density as a function of the scan rate for the different electrodes. E) Nyquist plots of NiCo-r, NiCo-p, and a bulk sample. F) Polarization curves after 1000 CV cycles with the NiCo-r electrode.

exhibited an OER performance that is superior to that of the reported Ir/C catalyst (20 wt%) in 1M KOH solution, thus confirming the beneficial role of oxygen vacancies and an ultrathin thickness in the OER process.

According to these results, the enhanced OER performance of nanosheets that are rich in oxygen vacancies can be attributed to the synergistic interplay of the number and reactivity of active sites, which results from the ultrathin thickness and presence of oxygen vacancies. First, the ultrathin nanosheet structures feature more active sites on their surfaces than their bulk counterparts, resulting in greatly facilitated surface reactions. Second, the introduction of oxygen vacancies in the ultrathin sheets decreases the energy required for the adsorption of H_2O molecules onto the surface, which in turn leads to an increase in the OER reaction rate. Lastly, the ultrathin thickness also leads to an intimate contact with the substrate electrode, a high interfacial contact area with the electrolyte, and short ion diffusion paths, thus ensuring good electron transport.

In summary, by taking spinel-structured nanosheets as an example, we have clearly identified the crucial roles of oxygen vacancies and an ultrathin thickness in the OER process, which were confirmed by both theoretical and experimental studies. In detail, the oxygen vacancies enhance the reactivity of the active sites, as they reduce the H_2O adsorption energy. Meanwhile, the ultrathin thickness of the nanosheets increases the number of active sites and thus facilitates reactions on the surface; therefore, the as-obtained nanosheets perform very well in water oxidation processes. Among the various spinel-structured nanosheets, the $NiCo_2O_4$ ultrathin nanosheets that were rich in oxygen vacancies exhibited a large current density of 285 $mA cm^{-2}$ at 0.8 V and a small overpotential of 0.32 V; both of these values are better than most values that have been reported for non-precious-metal OER catalysts. This study should thus provide guidelines for the future design of new electrode materials with optimized structures to improve the overall OER performance.

Experimental Section

Electrochemical measurements: All of the electrochemical measurements were performed in a three-electrode system on an electrochemical workstation (CHI660B). In brief, the catalyst (4 mg) was dispersed in a water/isopropanol solution (1 mL, 3:1 v/v) with 30 μL Nafion solution (Sigma Aldrich, 5 wt%) by sonicating for 40 min to form a homogeneous ink. Then, 5 μL of the dispersion (containing 20 μg of catalyst) was loaded onto a glassy carbon electrode with a diameter of 3 mm (loading 0.285 $mg cm^{-2}$). Finally, the as-prepared catalyst films were dried at room temperature. Linear sweep voltammetry with a scan rate of 5 $mV s^{-1}$ was carried out in 1M KOH solution using a Ag/AgCl electrode as the reference electrode, a Pt electrode as the counter electrode, and the glassy carbon electrode with various catalysts as the working electrode. Cyclic voltammetry (CV) was conducted from 0 to 0.8 V vs. Ag/AgCl to investigate the cycling stability. The Nyquist plots were measured with frequencies ranging from 100 kHz to 1 Hz, and the amplitude of the applied voltage was 5 mV. The impedance data were fitted to

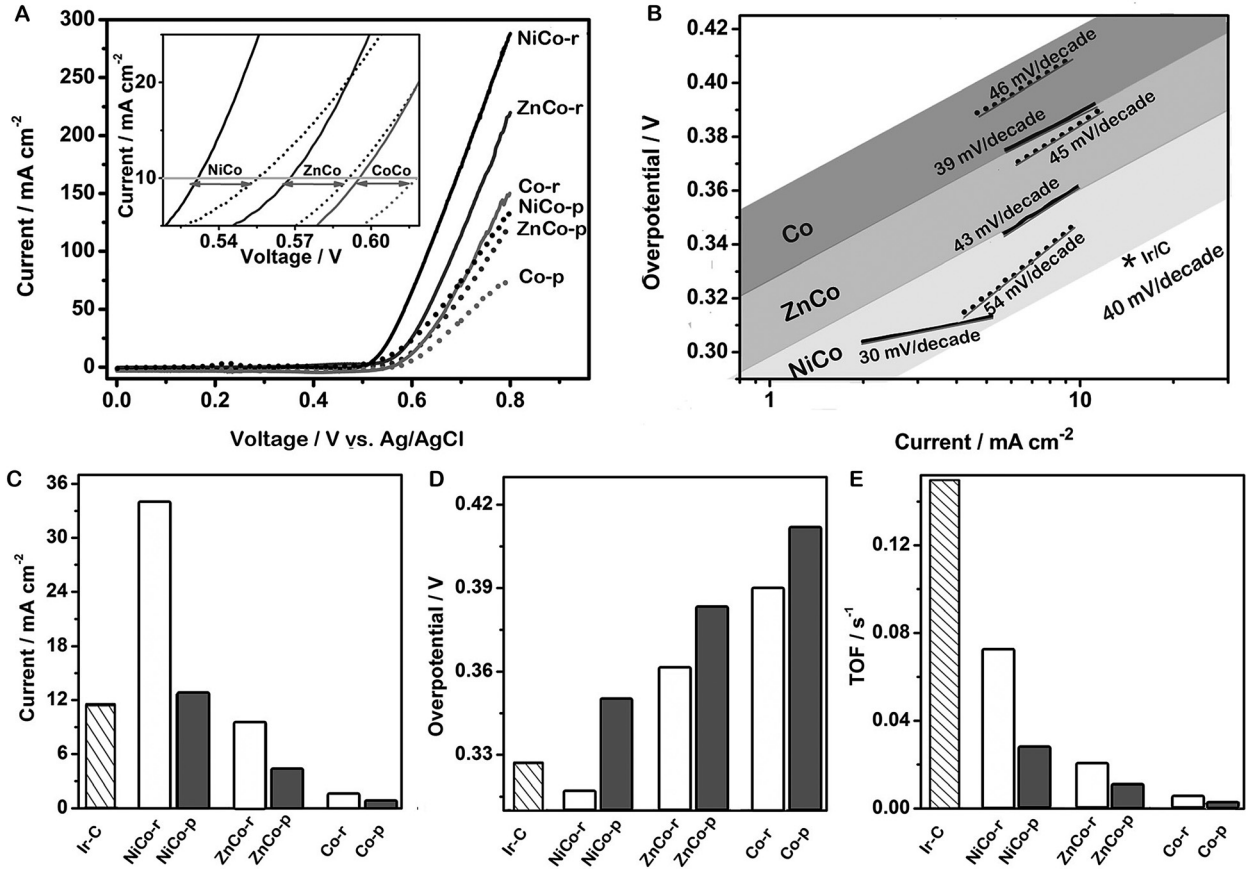

Figure 4. A) Polarization curves of the spinel-structured samples. Inset: enlargement of the region near the onset. B) Corresponding Tafel plots; —— and ••••• correspond to samples that are rich and poor in oxygen vacancies, respectively. Comparison of C) the current achieved at a potential of 0.57 V, D) the overpotential required for a current of 10 mA cm^{-2}, and E) the TOF values calculated from the current at $\eta = 0.36$ V for the tested samples and an Ir/C (20 wt%) catalyst as a reference.[31,32]

a simplified Randles circuit to extract the charge-transfer resistances. For more details, see the Supporting Information.

Keywords: electrocatalysis · heterogeneous catalysis · oxygen evolution reaction · oxygen vacancies · spinel phases

How to cite: *Angew. Chem. Int. Ed.* **2015**, *54*, 7399–7404
Angew. Chem. **2015**, *127*, 7507–7512

[1] B. Lim, M. Jiang, P. H. Camargo, E. C. Cho, J. Tao, X. Lu, Y. Zhu, Y. Xia, *Science* **2009**, *324*, 1302.
[2] B. Winther-Jensen, O. Winther-Jensen, M. Forsyth, D. R. MacFarlane, *Science* **2008**, *321*, 671.
[3] Z.-G. Ye, H.-M. Meng, D.-B. Sun, *Electrochim. Acta* **2008**, *53*, 5639.
[4] M. Gao, W. Sheng, Z. Zhuang, Q. Fang, S. Gu, J. Jiang, Y. Yan, *J. Am. Chem. Soc.* **2014**, *136*, 7077.
[5] J. Suntivich, K. J. May, H. A. Gasteiger, J. B. Goodenough, Y. Shao-Horn, *Science* **2011**, *334*, 1383.
[6] S. W. Lee, C. Carlton, M. Risch, Y. Surendranath, S. Chen, S. Furutsuki, A. Yamada, D. G. Nocera, Y. Shao-Horn, *J. Am. Chem. Soc.* **2012**, *134*, 16959.
[7] J. Wang, H. X. Zhong, Y. L. Qin, X. B. Zhang, *Angew. Chem. Int. Ed.* **2013**, *52*, 5248; *Angew. Chem.* **2013**, *125*, 5356.
[8] Y. Sun, S. Gao, F. Lei, J. Liu, L. Liang, Y. Xie, *Chem. Sci.* **2014**, *5*, 3976.
[9] J. B. Gerken, J. G. McAlpin, J. Y. Chen, M. L. Rigsby, W. H. Casey, R. D. Britt, S. S. Stahl, *J. Am. Chem. Soc.* **2011**, *133*, 14431.
[10] Y. Liang, Y. Li, H. Wang, J. Zhou, J. Wang, T. Regier, H. Dai, *Nat. Mater.* **2011**, *10*, 780.
[11] R. D. L. Smith, M. S. Prevot, R. D. Fagan, Z. P. Zhang, P. A. Sedach, M. K. J. Siu, S. Trudel, C. P. Berlinguette, *Science* **2013**, *340*, 60.
[12] Y. Wang, T. Zhou, K. Jiang, P. Da, Z. Peng, J. Tang, B. Kong, W. B. Cai, Z. Yang, G. Zheng, *Adv. Energy Mater.* **2014**, *4*, 1400496.
[13] Y.-H. Fang, Z.-P. Liu, *J. Am. Chem. Soc.* **2010**, *132*, 18214.
[14] F. Song, X. Hu, *Nat. Commun.* **2014**, *5*, 4477.
[15] F. Song, X. Hu, *J. Am. Chem. Soc.* **2014**, *136*, 16481.
[16] X. Zhang, Y. Xie, *Chem. Soc. Rev.* **2013**, *42*, 8187.
[17] X. Zhang, Q. Liu, L. Meng, H. Wang, W. Bi, Y. Peng, T. Yao, S. Wei, Y. Xie, *ACS Nano* **2013**, *7*, 1682.
[18] J. Bao, X. Zhang, L. Bai, W. Bai, M. Zhou, J. Xie, M. Guan, J. Zhou, Y. Xie, *J. Mater. Chem. A* **2014**, *2*, 10876.
[19] J. Rosen, G. S. Hutchings, F. Jiao, *J. Am. Chem. Soc.* **2013**, *135*, 4516.
[20] F. Cheng, T. Zhang, Y. Zhang, J. Du, X. Han, J. Chen, *Angew. Chem. Int. Ed.* **2013**, *52*, 2474; *Angew. Chem.* **2013**, *125*, 2534.
[21] G. Wu, N. Li, D.-R. Zhou, K. Mitsuo, B.-Q. Xu, *J. Solid State Chem.* **2004**, *177*, 3682.
[22] L. Liang, J. Zhang, Y. Zhou, J. Xie, X. Zhang, M. Guan, B. Pan, Y. Xie, *Sci. Rep.* **2013**, *3*, 1936.

[23] H. X. Wang, Z. A. Hu, Y. Q. Chang, Y. L. Chen, H. Y. Wu, Z. Y. Zhang, Y. Y. Yang, *J. Mater. Chem.* **2011**, *21*, 10504.
[24] J. Pu, J. Wang, X. Jin, F. Cui, E. Sheng, Z. Wang, *Electrochim. Acta* **2013**, *106*, 226.
[25] J.-G. Kim, D. Pugmire, D. Battaglia, M. Langell, *Appl. Surf. Sci.* **2000**, *165*, 70.
[26] X.-F. Lu, D.-J. Wu, R.-Z. Li, Q. Li, S.-H. Ye, Y.-X. Tong, G.-R. Li, *J. Mater. Chem. A* **2014**, *2*, 4706.
[27] T. Choudhury, S. Saied, J. Sullivan, A. Abbot, *J. Phys. D* **1989**, *22*, 1185.
[28] Y. E. Roginskaya, O. Morozova, E. Lubnin, Y. E. Ulitina, G. Lopukhova, S. Trasatti, *Langmuir* **1997**, *13*, 4621.
[29] V. Jiménez, A. Fernandez, J. Espinós, A. González-Elipe, *J. Electron Spectrosc. Relat. Phenom.* **1995**, *71*, 61.
[30] J. Xie, J. Zhang, S. Li, F. Grote, X. Zhang, H. Zhang, R. Wang, Y. Lei, B. Pan, Y. Xie, *J. Am. Chem. Soc.* **2013**, *135*, 17881.
[31] M. Gong, Y. Li, H. Wang, Y. Liang, J. Z. Wu, J. Zhou, J. Wang, T. Regier, F. Wei, H. Dai, *J. Am. Chem. Soc.* **2013**, *135*, 8452.
[32] X. Liu, J. Liu, Y. Li, Y. Li, X. Sun, *ChemCatChem* **2014**, *6*, 2501.

Received: March 10, 2015
Revised: April 11, 2015
Published online: May 7, 2015

